Design and Analysis of a Double Coaxial Magnetic Coupling to Improve Torque Density

Yusuf Akcay
Pemc Research Group
University of Nottingham
Nottingham, UK
yusuf.akcay1@nottingham.ac.uk

Oliver Tweedy
Pemc Research Group
University of Nottingham
Nottingham, UK
oliver.tweedy1@nottingham.ac.uk

Paolo Giangrande
Pemc Research Group
University of Nottingham
Nottingham, UK
p.giangrande@nottingham.ac.uk

Michael Galea
Key Laboratory of More Electric Aircraft
Technology of Zhejiang Province
University of Nottingham
Ningbo, China
michael.galea@nottingham.ac.uk

***Abstract*— Coaxial magnetic couplings are an attractive alternative to traditional mechanical machine couplings which bring several desirable advantages but are limited by their relatively low torque density and torque to mass ratio. The optimum magnetic design of a coaxial magnetic coupling possesses a significant volume of inactive material due to the radius of the permanent magnet arrays. In this paper, the torque density of a coaxial magnetic coupling is increased by up to 82% by utilizing a second set of permanent magnet rings to form a double coaxial magnetic coupling. The proposed design enhancement achieves the aim of reducing the total volume of the coupling, whilst maintaining the same mass and peak torque transmission capacity.**

Keywords—contactless torque transmission, finite element method, permanent magnet, magnetic couplings, analytical method

I. INTRODUCTION

Magnetic couplings (MCs) are traditionally employed where contactless power transmission is required between two or more machines, for example in wave turbine generators. Due to the nature of their operation, MCs provide passive overload protection, reduced maintenance requirements and misalignment tolerance, qualities which have resulted in more widespread adoption of magnetic couplings as their performance has improved over time, [1]-[2]. The main disadvantage of magnetic couplings stems from the low torque transfer capability of permanent magnets relative to that of physical rigid or flexible mechanical couplings. As a result, the torque to volume (torque density) and torque to mass ratio of magnetic couplings is lower than that of standard mechanical couplings which limits their use in applications where weight and volume savings are critical (such as in aerospace). In addition, magnetic couplings require softer starting conditions with more gradual torque ramps and/or lower inertia of connected machines.

Magnetic couplings commonly appear in either an axial or radial configuration, with the latter providing a greater peak torque holding capacity. Radial / coaxial magnetic couplings are essentially the same as a magnetic gear with a ratio of one-to-one, with the physical interaction between teeth replaced with the interlocking magnetic fields between opposing permanent magnets (PMs).

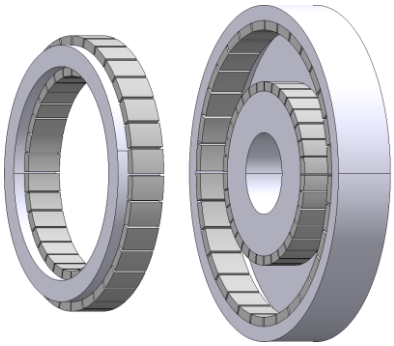

Fig. 1. Overview of the double coaxial magnetic coupling.

Current research into magnetic couplings is driven by the need to develop solutions that improve the torque density and torque to mass ratio. The general aim of such research is to bring the benefits of magnetic power transmission to aerospace and automotive applications without significantly reducing vehicle performance and efficiency. An important first step in designing a magnetic coupling is to identify and optimise the size parameters that determine the scale and position of the permanent magnets and back iron in the structure. The finite element method (FEM) can be used to determine the optimum size parameters, [3]-[4]. But given the high number of potential combinations of size parameters, the process of setting up and running FEM simulations can become time consuming and complicated. Instead, an analytical method is used to establish the initial geometry of the coupling.

The methodology used in this paper is based on the analytical techniques described in the following research. A method of obtaining the exact solution for the magnetic field distribution and electromagnetic torque in an axial coupling is demonstrated by Thierry et al [5] with a 2D analytical model based on subdomain analysis Further to this, the static torque distribution of a coaxial magnetic coupling is shown to be obtainable via the analytical method shown in [6].

Yao et al [7] explores the effect of air gap length in coaxial magnetic couplings and provides a comparison between 3D FEM and 2D results. Several size parameters are considered when the analytical 2D analysis model is adopted, and such degree of flexibility is difficult to achieve through the 3D FEM approach. In this paper a double magnetic coupling (DMC) is designed and optimised. The torque to

volume and torque to mass ratio of the coupling are compared with a single magnetic coupling (SMC) and the advantages and disadvantages of the double coaxial configuration are discussed.

II. The Proposed DMC

The proposed DMC geometry aims to reduce the total coupling volume whilst maintaining the same or improved torque holding capacity. High performance magnetic coupling designs target high reliability while having less volume/size of designs. In this section, the overview of the proposed coupling with its size parameters are detailed. The section then continues by giving a 2D analytical representation for a trade-off study and details the optimal combination of size parameters that produce the greatest torque to volume ratio for permanent magnets in a DMC. The resulting change in torque to mass ratio is also obtained.

A. General overview and size parameters of the DMC

The DMC is comprised of two sets of PMs on both motor and load sides. This configuration makes use of the available space within the inner magnet core of the single coaxial geometry. The compact design of the double coaxial structure fills the same cylindrical volume as the SMC at the expense of increasing the total mass. However, the relative increase in torque density is significantly greater than the relative reduction in torque to mass ratio. The overview of the rotors on motor/load sides are given in Fig. 2. The 2D analytical representation of the DMC is created by using the geometrical parameters within the subdomains detailed in Fig. 3. According to the equivalent representation of the DMC given in Fig. 2b, the 2D analytical method evaluates the size parameters by having two identical rotors with only radial differences. Thus, the method proposed in [8] is used for the trade-off analysis. The size parameters are named in Table I.

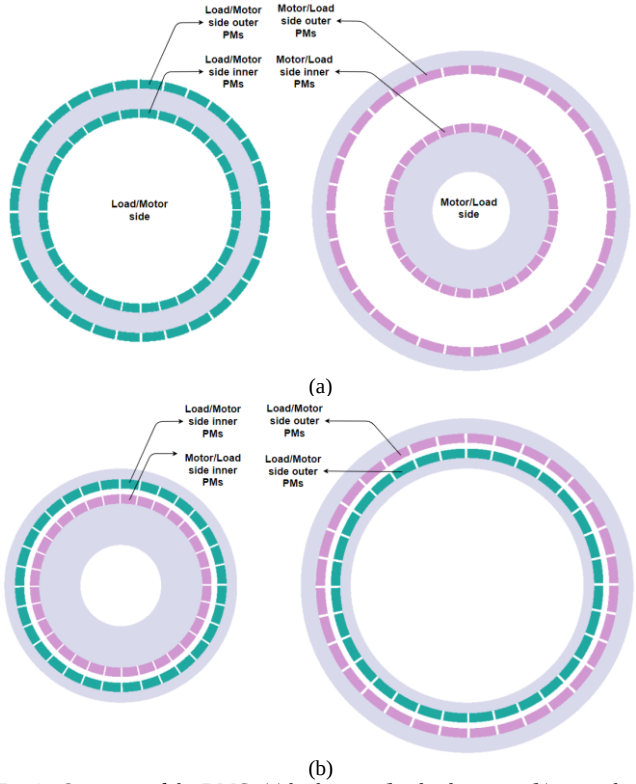

Fig. 2. Overview of the DMC; (a) both motor/load side rotors, (b) equivalent structure for the 2D analytical evaluation.

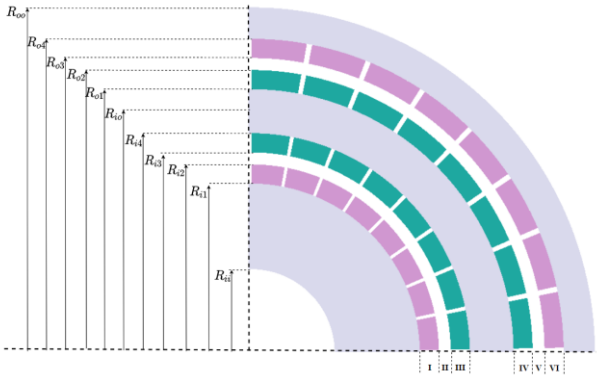

Fig. 3. Parameters of the couplings.

TABLE I. Size Parameters of the DMC

Symbol	Parameters
R_{ii}	Motor/Load side Inner Core Radius
R_{i1}	Motor/Load side Inner PM Inner Radius
R_{i2}	Motor/Load side Inner PM Outer Radius
R_{i3}	Load/Motor side Inner PM Inner Radius
R_{i4}	Load/Motor side Inner PM Outer Radius
R_{o1}	Load/Motor side Outer PM Inner Radius
R_{o2}	Load/Motor side Outer PM Outer Radius
R_{o3}	Motor/Load side Outer PM Inner Radius
R_{o4}	Motor/Load side Outer PM Outer Radius
R_{oo}	Motor/Load side Outer Core Radius
l_a	Axial Length

B. Analytical implementation

As explained in the previous sub-section, the equivalent representation for the 2D analysis is shown in Fig. 2b. Based on this configuration, the proposed MC can essentially be analysed as two separate magnetic couplings, a smaller inner coupling and a larger outer coupling. Thus, the DMC consists of three subdomains on each coupling parts and six subdomains in total. These are the inner (I) and outer (III) PMs, and the airgap (II) subdomains on the inner rotor, the inner (IV) and outer (VI) PMs, and the outer airgap (V) as shown in Fig. 3. The analytical method used in this paper accepts some assumptions such as no consideration of end effects, infinite permeability in the back iron, and the PMs have constant permeability and remanent flux density with a radial magnetization pattern.

The analytical method shown in [9-10] can be used for any type of magnetic coupling design, including the DMC. The equivalent representation of the DMC consists of two radial magnetic couplings. The analytical method takes the outer radius of the inner MC as an inner back-iron radius (R_{io}). The reference point is the outer radius (R_{oo}). The PM, back-iron and airgap thicknesses are always constant at 4 mm, 5 mm and 2.5 mm respectively. The optimum combination of size parameters for the outer MC is determined using the analytical method, these parameters determine the outer radius of the inner MC which is used as a fixed reference point for the inner MC analysis. Finally, the peak torque capacity is obtained after the size parameters for the inner MC are fixed. It should be noted that the back-iron thickness is selected prior to the use of the analytical method, this value is based on the saturation results obtained from a separate 2D FEM analysis.

C. Saturation observation

The analytical method used here assumes infinite iron core permeability, making it impossible to see any saturation effects. The proposed DMC includes three iron-cores; i.e. outer, middle and inner iron cores. The material used in the DMC's iron cores is stainless steel (grade 416) with a saturation knee point of 1.5 T. The finite element simulations for this analysis run on the Simcentre MagNet FE software package in a static 2D solver with linear material properties. This sub-section observes the effects of the number of pole-pairs ($\boldsymbol{p}$) on the back-iron field and plots the saturated area depending on the probe position in the back-iron. A single radial MC with size parameters given in Table II has been selected for saturation observation. The first analysis keeps the back-iron, airgap, and PM thicknesses constant, and varies the probe position in the back-iron and the pole-pair number. Fig. 4 demonstrates the saturated areas on the back-iron by using a threshold point of 1.5 T. The green areas show where the flux density probe readings are below saturation and are less than 1.5 T. The area in red highlights the saturated points. The highest flux density values are observed between a 30 mm to 55 mm radius.

The analysis has been repeated with different pole-pair numbers between 2 and 40 with 1 pole-pair difference. It is evident that the saturation can be easily avoided at higher pole-pair numbers (i.e. pole-pairs 14 and higher). However, if the design uses less than 14 pole-pairs, there will be saturation in the back-iron near the PMs. In that case, either the PM thickness must be reduced, or the airgap thickness must be increased. Fig. 5 shows the effects of PM thickness on the back-iron saturation. The airgap thickness and pole-pair number are kept constant at 4 mm and 3, respectively. Pole-pair number is selected due to long saturation area shown in Fig. 4. On the other hand, Fig. 6 depicts the effects of the airgap thickness on the saturation. In this analysis, the airgap thickness varies while the PM thickness and pole-pair numbers are fixed at 4 mm and 3, respectively. As mentioned before, the airgap and PM thickness are fixed at 2.5 mm and 4 mm in this paper. Thus a 5 mm back-iron thickness safely avoids any saturation and ensures mechanical integrity. Fig. 4 provides the reference points for the analytical method to correctly select the back-iron thickness when the pole-pair number is less than 14.

TABLE II. SIZE PARAMETERS OF THE SATURATION ANALYSIS

Symbol	1st Analysis (Fig. 4)	2nd Analysis (Fig. 5)	3rd Analysis (Fig. 6)
$\boldsymbol{R_{i1} - R_{ii}}$	25 mm	25 mm	25 mm
$\boldsymbol{R_{i2} - R_{i1}}$	4 mm	**varies**	4 mm
$\boldsymbol{R_{i2} - R_{i1}}$	2.5 mm	4 mm	**varies**
$\boldsymbol{B_m}$	95%	95%	95%
$\boldsymbol{R_{io}}$	69.5 mm	69.5	69.5
$\boldsymbol{l_s}$	40 mm	40 mm	40 mm
$\boldsymbol{p}$	**varies**	3	3

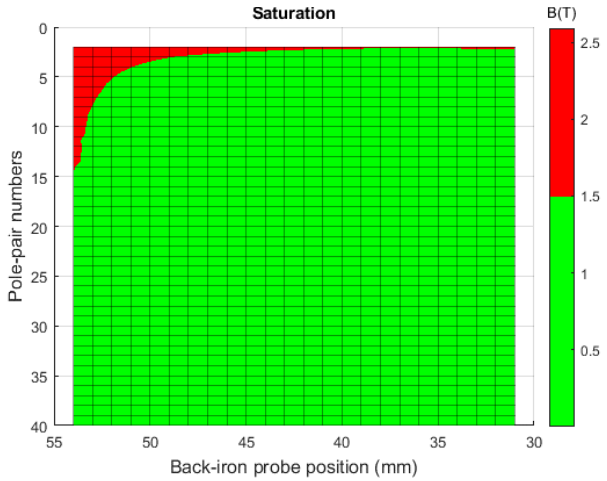

Fig. 4. Saturation considering back iron-thickness versus pole-pair number.

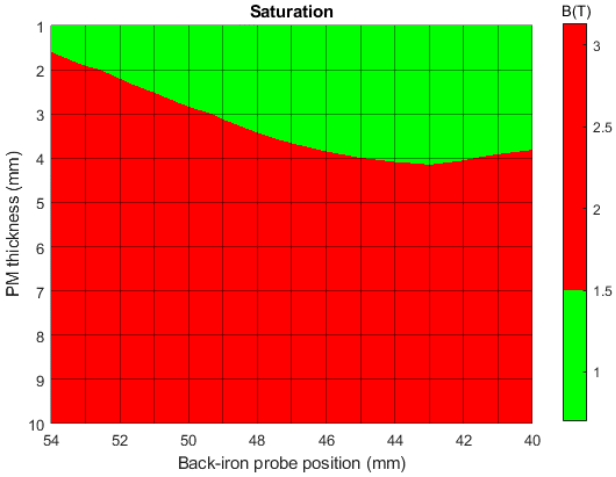

Fig. 5. Saturation considering PM thickness with 3 pole-pairs.

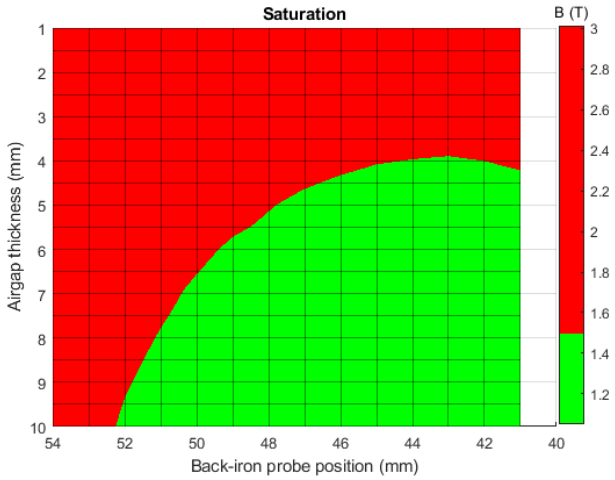

Fig. 6. Saturation considering airgap thickness at 3 pole-pairs.

III. TRADE-OFF STUDY AND COMPARATIVE ANALYSIS

The aims of the sensitivity analysis are to observe the torque holding capacity of the proposed DMC as a function of pole-pairs number and outer radius and to make a comparison with its single coaxial counterpart in terms of torque density considering the total volume and PM volume separately.

The analyses allow for the selection of parameters that produce the greatest torque density. As shown by the saturation analysis, the 2D analytical method progresses by avoiding saturation according to the data given in Figs. 4, 5 and 6. The PM and airgap thicknesses are 4 mm and 2.5 mm throughout the analyses. The active part length is fixed at 40 mm.

A. Torque density comparison considering the total volume

The torque density comparison considering the total volume of the double and single coaxial MCs are depicted in Figs. 7 and 8. The total volume is defined by a cylinder with the outer radius (R_{io}) and active part length (l_s). The trade-off analysis is performed taking into account pole-pair numbers between 2 and 40, and outer radius values between 60 mm and 200 mm. Since the PM, airgap and back-iron thicknesses are held constant, the value of the outer radius decides the inner MC's outer radius (R_{io}). The 2D analytical method automatically detects the latter radius (R_{io}) for the DMC. Fig. 7 clearly shows that the torque per total volume is greatly improved for the DMC. The torque density can be increased by up to 82% of the maximum value for the DMC. The data shows that the outer radius significantly effects the torque density as the larger outer radius allows for increased torque holding capacity in the inner rotor. This improvement means that a design with the double coaxial configuration can transfer the same torque as a single coaxial MC but in a significantly reduced volume.

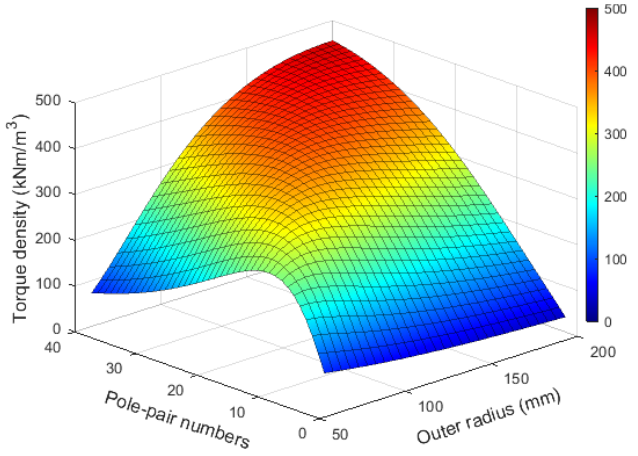

Fig 7. Torque density values by changing pole-pair number and outer radius of the DMC. (Torque per total volume).

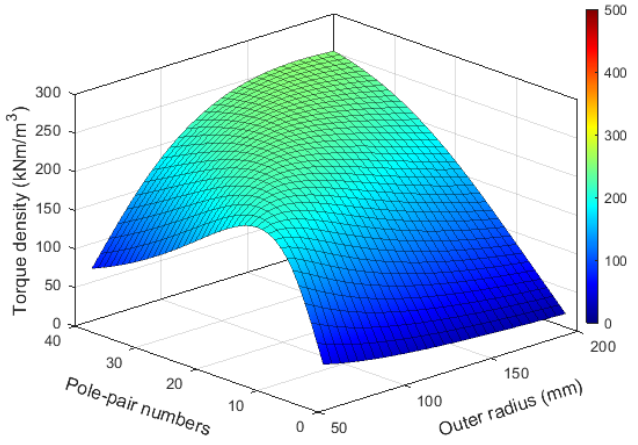

Fig.8. Torque density values by changing pole-pair number and outer radius of the SMC. (Torque per total volume)

B. Torque density comparison considering the PM volume

Another trade-off study is made by considering the torque per PM volume only. The DMC geometry is simplified to the four rings of PM magnets, with their volumes represented as four hollow cylinders. The inner coupling has two volumes defined by $\boldsymbol{R_{i2} - R_{i1}}$ and $\boldsymbol{R_{i4} - R_{i3}}$, and the outer coupling has two volumes defined by $\boldsymbol{R_{o2} - R_{o1}}$ and $\boldsymbol{R_{o4} - R_{o3}}$. The SMC on the other hand takes only the outer rings of PMs with two hollow cylinders defined by $\boldsymbol{R_{o2} - R_{o1}}$ and $\boldsymbol{R_{o4} - R_{o3}}$. Similarly, the analyses consider the pole-pair numbers between 2 and 40, while the outer radius ranges between 60 mm and 200 mm. The torque per PM volume is shown in Figs. 9 and 10 for the DMC and SMC, respectively. The figures clearly show that there is no significant difference in torque density for any value of pole-pair numbers and outer radius. It should be noted that the PM openings (i.e. the gaps between PMs due to the core teeth) are included in the hollow cylinder volumes of PMs. Based on the analyses shown in Figs. 9 and 10, another comparative analysis is performed to show the difference in the torque to mass ratio for the just the PMs between the DMC and SMC, the results of this analysis are shown in Fig. 11. The analysis aims to provide an understanding of both the advantages and disadvantages of the DMC. The figure shows the differences in torque per PM mass (i.e. in Nm/kg). It can be seen in Fig. 11 that although the torque density considering the total volume can be increased by up to 82%, more PM mass may be required to achieve the same amount of torque.

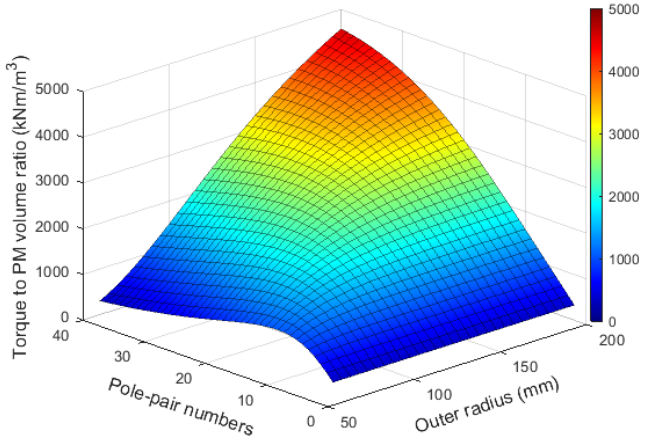

Fig. 9. Torque density values by changing pole-pair number and outer radius of the DMC. (Torque per PM volume).

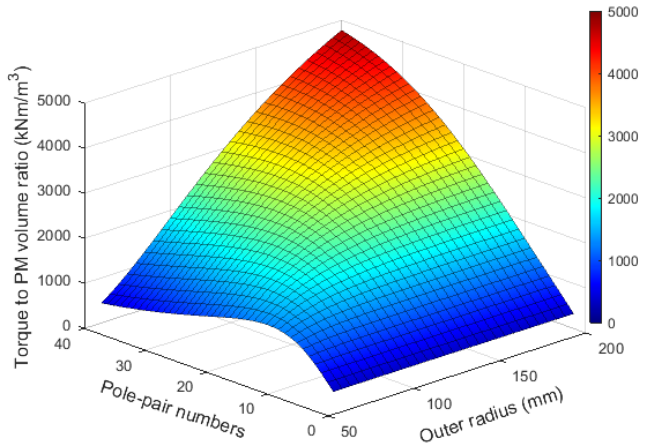

Fig. 10. Torque density values by changing pole-pair number and outer radius of the SMC. (Torque per PM volume).

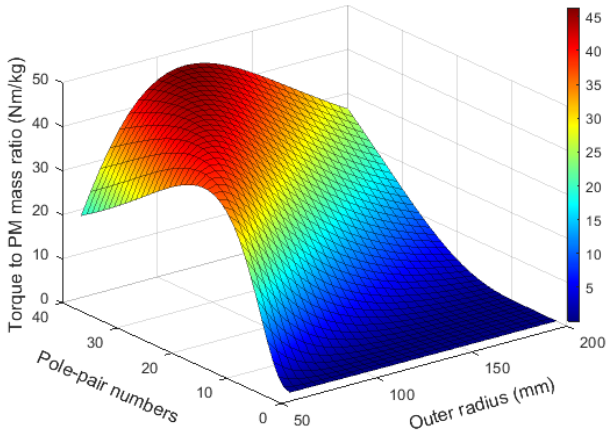

Fig. 11. Torque density difference between the DMC and SMC considering only PM mass in kg. (Torque per PM mass).

C. Static torque performance

This sub-section summarises the reason behind the increase in torque per PM mass on the proposed DMC. Two MCs from the data obtained in the previous sub-section have been selected with identical parameters. The PM, airgap, and back-iron thicknesses are 4 mm, 2.5 mm, and 5 mm, respectively for both couplings. The outer radius and the active part length are 90 mm and 40 mm respectively. A 90 mm outer radius makes the outer radius of the inner coupling of the DMC 69.5 mm. Based on the selected parameters, the torque results with respect to pole-pair numbers are shown in Fig. 12. The best torque value is obtained at 20 pole-pairs on the outer coupling. It should be noted that the outer parts are identical in both coupling configurations (i.e. the DMC and SMC). Thus, the SMC is also giving the optimum torque value at 20 pole-pairs. It should be noted that the inner rotor produces better torque when the pole-pair number is 15. The torque improvement is 12.3 Nm which is around 5.8% more torque. However, due to the outer rotor's static torque response, the inner part should have the same pole-pair number. This is due to the static torque period changing with the pole-pair number.

Fig. 13 shows the static torque responses over the angular shift between PMs for each coupling separately, and for both DMC and SMC configurations. The 15-20 pole-pair combination is not suitable as the static torque on the second half reduces significantly whereas 20-20 pole-pair combination have the same static torque period and contribute greatly to the overall torque. The MC with 15 pole-pair number has a period of 24 mechanical degrees, while 20 pole-pair number has 18 mechanical degrees. As the inner and outer MCs share the same angular displacement, only one MC will be positioned at the angular position that achieves peak static torque when the pole-pair number is different between MCs.

The dashed red line in Fig. 13 shows the static torque response on the SMC. The DMC can transfer 216 Nm more torque compared to the SMC with the same volume. The dashed-black line represents static torque for the inner coupling of the DMC with an outer radius (R_{io}) of 69.5 mm.

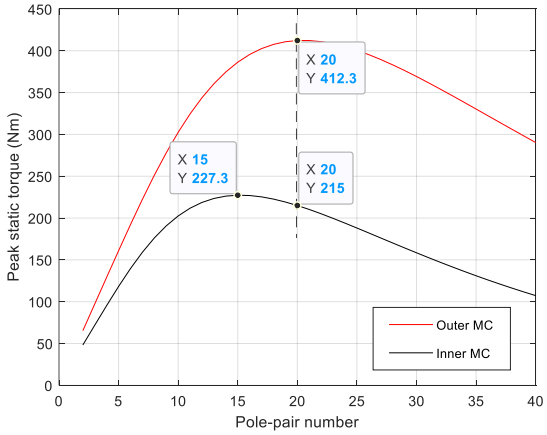

Fig.12. FEM results considering a 90 mm outer radius.

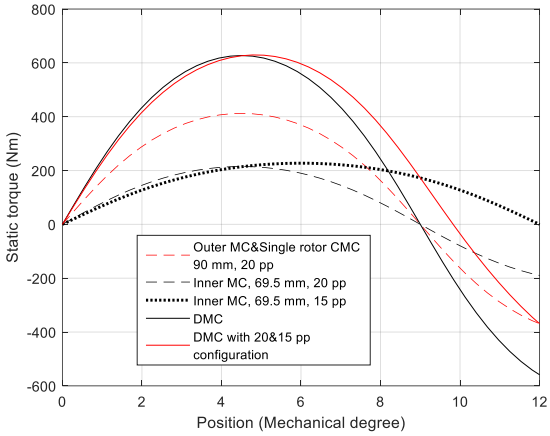

Fig. 13. Static torque distribution on the coupling parts.

D. Direct comparison between DMC and SMC

A new MC configuration with an increased torque per unit volume has been proposed. However, as a result, the total mass of the PMs in the new configuration was increased. To make a fair comparison between the DMC and SMC configurations, a 100 Nm torque is set as the target value for both MC configurations. The fixed parameters that achieve this target torque are given in Table III. The active length of both couplings is changed to reach the target value.

TABLE III. 100 NM COUPLINGS SIZE PARAMETERS

Symbol	DMC	SMC
l_a	2.5	2.5
p	20	20
l_m	4 mm	4 mm
l_b	5 mm	5 mm
B_m	95%	95%
l_{out}	90	90

The summary of the comparative analysis for the 100 Nm target value is shown in Table IV. The active lengths required to achieve the target torque are obtained as 8 mm and 13 mm for the DMC and SMC respectively. The total mass and PM mass are both 7% larger for the DMC. The torque density considering torque per total volume is increased by 62% for the DMC while the torque per PM mass value is reduced by 6%. The percentage change stays the same when considering

torque per total mass. The outer radius (R_{oo}) considerably affects the torque per total volume. As shown in the previous sub-section, a larger radius can lead to an increased torque density, which can be as high as 82%.

TABLE IV. 100 NM COUPLINGS RESULTS

Definition	DMC	SMC
Active length (l_s)	8 mm	13 mm
PM mass	0.4 kg	0.37 kg
Core mass	0.54 kg	0.51 kg
Total mass	0.94 kg	0.88 kg
Torque per PM mass	251 Nm/kg	268 Nm/kg
Torque per total mass	106.4 Nm/kg	114.14 Nm/kg
Torque per PM volume	1790 kNm/m3	1919 kNm/m3
Torque per total volume	491.2 kNm/m3	302.3 kNm/m3

The flux density distributions of both DMC and SMC are given in Fig. 14. The plots show that a 5 mm back-iron thickness avoids any saturation on both couplings. Both MCs (designed for 100 Nm) are also compared in terms of axial force and separation distance should the complete disconnection of the inner and outer rings be required.

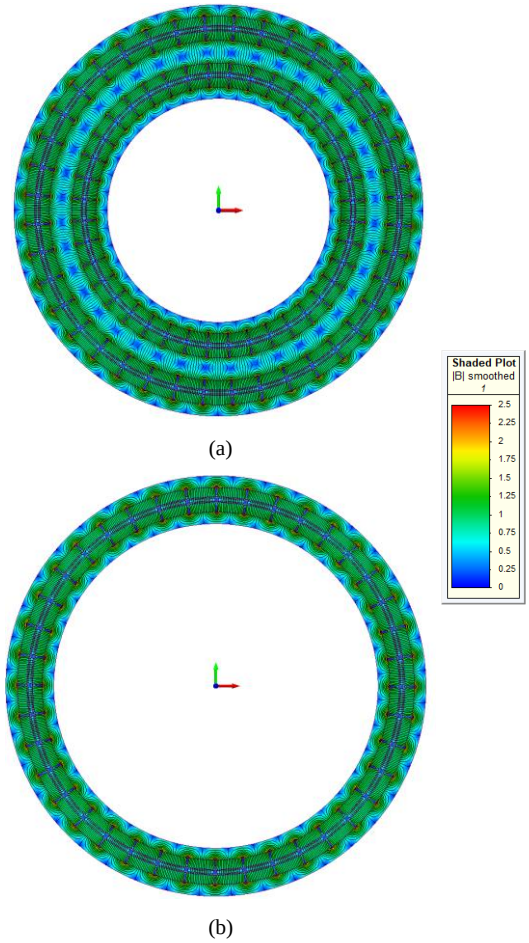

(a)

(b)

Fig. 14. Flux density distributions of the DMC (up) and SMC (bottom).

IV. CONCLUSIONS

A double coaxial magnetic coupling is designed and optimised with the use of a 2D analytical method. The proposed design achieves the objective of increasing the torque density of a coaxial magnetic coupling with a small reduction in torque to mass ratio. The torque density of the MC is increased by a maximum of 82% and the torque to mass ratio is reduced by 6%. In a practical case study comparing the DMC to an SMC with the same torque capacity, the torque per total volume is increased by 62%.

Future development of such a design must consider the geometry of the supporting rotor structures which can represent a significant proportion of the coupling's mass if not designed with maximizing the torque to mass ratio in mind.

V. ACKNOWLEDGEMENT

This project received funding from the Clean Sky 2 Joint Undertaking under the European Union's Horizon 2020 research and innovation programme under grant agreements no 821023 and no. 807081. This work was also partially funded by the University of Nottingham Propulsion Futures Beacon.

References

[1] J. -. Yonnet, S. Hemmerlin, E. Rulliere and G. Lemarquand, "Analytical calculation of permanent magnet couplings," in IEEE Transactions on Magnetics, vol. 29, no. 6, pp. 2932-2934, Nov. 1993.

[2] W. Wu, H. C. Lovatt and J. B. Dunlop, "Analysis and design optimisation of magnetic couplings using 3D finite element modelling," in IEEE Transactions on Magnetics, vol. 33, no. 5, pp. 4083-4094, Sept. 1997.

[3] S. Mezani, B. Laporte, and N. Takorabet, "Saturation and space harmonics in the complex finite element computation of induction machine," IEEE Trans. Magn., vol. 41, no. 5, pp. 1460–1463, May. 2005.

[4] A. Al-Timimy, M. Al-Ani, M. Degano, P. Giangrande, C. Gerada, and M. Galea, "Influence of rotor endcaps on the electromagnetic performance of high-speed PM machine," IET Electr. Power Appl., Mar. 2018.

[5] T. Lubin, S. Mezani and A. Rezzoug, "Simple Analytical Expressions for the Force and Torque of Axial Magnetic Couplings," in *IEEE Transactions on Energy Conversion*, vol. 27, no. 2, pp. 536-546, June 2012.

[6] M.H. Nagrial, "Analysis design and performance of magnetic couplings", Proc. IEEE International Conference on Power Electronics and Drive Systems (PEDS'95), *vol. 21–24*, pp. 634-638, February 1995.

[7] Y. D. Yao, D. R. Huang, S. M. Lin, S. J. Wang, "Theoretical computations of the magnetic coupling between magnetic gears", IEEE Trans. Magn., vol. 32, pp. 710-713, 1996.

[8] Y. Akcay, P. Giangrande, O. Tweedy, and M. Galea, "Fast and Accurate 2D Analytical Subdomain Method for Coaxial Magnetic Coupling Analysis" *Energies* 14, no. 15: 4656, 2021.

[9] T. Lubin, S. Mezani and A. Rezzoug, "Exact Analytical Method for Magnetic Field Computation in the Air Gap of Cylindrical Electrical Machines Considering Slotting Effects," in *IEEE Transactions on Magnetics*, vol. 46, no. 4, pp. 1092-1099, April 2010.

[10] T. Lubin, S. Mezani and A. Rezzoug, "Analytical Computation of the Magnetic Field Distribution in a Magnetic Gear," in *IEEE Transactions on Magnetics*, vol. 46, no. 7, pp. 2611-2621, July 2010.